

# Three-qubit topological phase on entangled photon pairs

Markus Johansson<sup>1</sup>, Antonio Z. Khoury<sup>2</sup>, Kuldip Singh<sup>1</sup> and Erik Sjöqvist<sup>1,3</sup>

<sup>1</sup> *Centre for Quantum Technologies, National University of Singapore, 3 Science Drive 2, 117543 Singapore, Singapore*

<sup>2</sup> *Instituto de Física, Universidade Federal Fluminense, 24210-346 Niterói - RJ, Brazil and*

<sup>3</sup> *Department of Quantum Chemistry, Uppsala University, Box 518, SE-751 20 Uppsala, Sweden*

We propose an experiment to observe the topological phases associated with cyclic evolutions, generated by local  $SU(2)$  operations, on three-qubit entangled states prepared on different degrees of freedom of entangled photon pairs. The topological phases reveal the nontrivial topological structure of the local  $SU(2)$  orbits. We describe how to prepare states showing different topological phases, and discuss their relation to entanglement. In particular, the presence of a  $\pi/2$  phase shift is a signature of genuine tripartite entanglement in the sense that it does not exist for two-qubit systems.

PACS numbers: 03.65.Vf, 03.67.Mn, 07.60.Ly, 42.50.Dv

## I. INTRODUCTION

Topological phases of quantum systems that evolve in topologically nontrivial spaces, have attracted considerable attention in a wide variety of subdisciplines in modern physics. Perhaps the most well-known example of such a topological quantity is the Aharonov-Bohm phase acquired by a charged particle that encircles a shielded magnetic flux line [1]. This phase depends only on the winding number of the particle's path around the impenetrable region of magnetic flux, but it is insensitive to perturbations of the path.

A topological phase acquired by a pair of entangled qubits undergoing cyclic local unitary evolution has been discovered [2]. The topological interpretation of this phase relies on the relation between two-qubit states and the rotation group  $SO(3)$  [3]. This is perhaps most clearly seen in the case of the maximally entangled states. These states are in one-to-one correspondence with the points of real projective space  $S^3/Z_2 \sim SO(3)$  [4, 5]. The two possible topological phases 0 and  $\pi$  can be associated with the two homotopy classes of loops in  $SO(3)$ . In other words the accumulated phase is not affected by continuous deformations of path of the cyclic evolution. The topological two-qubit phase has been observed in spin-orbit transformations on a laser beam [6] and in a nuclear magnetic resonance setting [7].

The notion of topological phase has been extended to pairs of entangled higher-dimensional quantum systems [8]. These phases are integer multiples of  $2\pi/d$ , where  $d$  is the Hilbert space dimension of each subsystem. Thus, for such objects, fractional values may occur. The topological phase for a given cyclic local  $SU(d)$  evolution of a state  $|\psi\rangle = \sum_{k,l=1}^d \alpha_{kl} |kl\rangle$  is restricted by the invariance of the determinant  $\det \alpha_{kl}$  of the coefficient matrix. Since  $\det \alpha_{kl} = 0$  for product states, the topological phase is only well-defined in the presence of entanglement.

Recently, the notion of topological phase has been extended to  $N$ -qubit systems [9]. These multi-qubit phases may take fractional values for  $N \geq 3$ . The number of possible values increases rapidly with the number of

qubits. All possible values for up to  $N = 7$  have been found using a combinatorial algorithm [9]. Furthermore, a relation between the topological phases and the degree of nonzero polynomial entanglement invariants has been conjectured [9]. As an example of such a relation, the possible topological phases  $0, \pi/2, \pi$ , and  $3\pi/2$  for  $N = 3$  can be linked to multipartite entanglement in the sense that three-tangle is a polynomial invariant of degree  $n = 4$ , namely the hyperdeterminant in the coefficient matrix  $\alpha_{klm}$  [10]. This implies that the allowed topological phases are indeed restricted to integer multiples of  $2\pi/n = \pi/2$ .

In order to realize a multiple qubit system in a photonic device, one may combine different degrees of freedom that can be manipulated independently. Numerous experiments have employed polarization and orbital angular momentum (OAM) to implement controlled operations [11–15] and spin-orbit Bell inequality [16, 17]. Here, we propose an experiment to measure the topological phases for  $N = 3$ , in qubits encoded on photon pairs produced by spontaneous parametric down conversion (SPDC). Each photon carries a polarization and orbital degree of freedom. The three qubits are encoded in the orbital part of the signal photon and the two polarizations, by projecting the orbital part of the idler photon on a well-defined Laguerre-Gaussian mode. In this way, we demonstrate different three-qubit states that acquire the different three-qubit phases by employing local  $SU(2)$  transformations in Franson loop interferometers on each photon. The observed phases would be a signature of the local orbits and thereby a non-trivial signature of multipartite entanglement.

The outline of the paper is as follows. The theory of topological three-qubit phases arising in local  $SU(2)$  evolution is described in Sec. II. Sections III–V contain the experimental setup, where the generation of three different types of three-qubit states are described in Sec. III, the measurement of topological phases is described in Sec. IV, and examples of evolutions that reveal the topological phases is given in Sec. V. The paper ends with the conclusions.

## II. THREE-QUBIT TOPOLOGICAL PHASE STRUCTURE

When considering interconvertibility of three-qubit states under stochastic local operations and classical communication (SLOCC), the genuinely tripartite entangled states fall into two classes [18]. These classes are termed the GHZ-class and the W-class after their representatives, the GHZ state and the W state.

By considering interconvertibility under local unitary transformations the two SLOCC-classes can be further divided into local unitary classes, or in other words, orbits of the group of local unitary transformations. The structure of such an orbit constitutes a qualitative description of the entanglement of the states belonging to the orbit. This is the most detailed description of the entanglement properties that can be given [19]. Since the action of the  $U(1)$  group is a trivial global phase shift, it is sufficient to consider the local  $SU(2)$ -orbits to study entanglement properties.

The structure of the  $SU(2)$ -orbits of entangled three-qubit states has been studied by Carteret and Sudbery in Ref. [20]. In particular it was shown that the local  $SU(2)$ -orbit of a GHZ state  $|\psi_{ghz}\rangle = \frac{1}{\sqrt{2}}(|++\rangle + |--\rangle)$ , where  $|+\rangle$  and  $|-\rangle$  are orthogonal states, is quadruply connected. The four different homotopy classes of cyclic evolutions correspond to the four different accumulated phases,  $0, \frac{\pi}{2}, \pi$  and  $\frac{3\pi}{2}$ . Since these are the only phases allowed for a state with nonzero three-tangle it follows that the quadruple connectedness is related to the tripartite entanglement measured by the three-tangle. A  $\frac{\pi}{2}$  phase shift cannot be generated in a two-qubit system and is therefore a measurable quantity that indicates the presence of tri-partite entanglement.

Four different topological phases is in fact not the most common topological phase structure for local  $SU(2)$ -orbits belonging to the GHZ SLOCC-class. Using the canonical form of three-qubit states of Carteret *et al.* [21], it can be seen that the set of local  $SU(2)$  orbits that exhibit four topological phases forms a subset of the local  $SU(2)$  orbits of the GHZ SLOCC-class parameterized by four real parameters, while the full set of local  $SU(2)$  orbits is parameterized by four real and one complex parameter. The states of this subset can, up to local  $SU(2)$  operations, be written on the form

$$|X_{a,b,c,d}\rangle = a|+++\rangle + b|+-\rangle + c|-+-\rangle + d|---\rangle, \quad (1)$$

where  $a, b, c, d \in \mathbb{C} \setminus \{0\}$  such that  $|a|^2 + |b|^2 + |c|^2 + |d|^2 = 1$ . We will refer to this class of states as the X-class. A distinguished member of this class is the three-qubit state  $|\psi_X\rangle$  for which  $a = b = c = d = \frac{1}{2}$  termed the three-qubit X state in Ref. [22]. This state is maximally entangled in the sense that all reduced density operators for the individual qubits are proportional to the identity. Note that the X state can be brought to the GHZ state by application of a Hadamard transformation on each

qubit. Hence, these two states are entangled in exactly the same way.

The states in the GHZ SLOCC-class that do not fall in the X-class have only two different topological phases. Since the X-class is a lower dimensional subset, a generic state in the GHZ SLOCC-class is of this kind. An example of such a state, with a doubly connected local  $SU(2)$  orbit, is a biased GHZ state  $|\psi_{bghz}\rangle = \alpha|+++\rangle + \beta|---\rangle$ , where  $|\alpha| \neq |\beta|$  and  $|\alpha|^2 + |\beta|^2 = 1$  [20]. The two homotopy classes of cyclic evolutions correspond to the accumulated phases  $0$  and  $\pi$ .

The X state and a biased GHZ state thus represents the two different topological phase structures present in the GHZ SLOCC-class. The remaining three-qubit states with genuine tripartite entanglement belong to the W SLOCC-class, and have either the topological phases  $0$  and  $\pi$ , or no topological phases at all. We would thus not see any other sets of topological phases by studying states in the W class.

This paper is concerned with three-qubit systems encoded in the polarization and orbital angular momentum (OAM) states of photons. We will be describing the polarization states in a basis of right and left circular polarization states  $|+\rangle$  and  $|-\rangle$  or alternatively in a basis of horizontal and vertical polarization states  $|H\rangle$  and  $|V\rangle$ . The relation between these basis vectors is given by  $|\pm\rangle = \frac{1}{\sqrt{2}}(|H\rangle \pm i|V\rangle)$ . The OAM states will be described in terms of a basis of Laguerre-Gaussian modes of first order  $LG_{1,0}$  and  $LG_{-1,0}$ , denoted  $|+\rangle$  and  $|-\rangle$  similarly to the circular polarization states, or in a basis of the Hermite-Gaussian first order modes  $HG_{1,0}$  and  $HG_{0,1}$ , denoted  $|h\rangle$  and  $|v\rangle$  similarly to the linear polarization states. The relation between these bases is given by  $|\pm\rangle = \frac{1}{\sqrt{2}}(|h\rangle \pm i|v\rangle)$ .

It is useful to note that the X state prepared in a basis of circular polarization states and Laguerre-Gaussian modes is the GHZ state, up to a relative phase factor  $-i$  of the two terms, in a basis of horizontal and vertical polarization states and Hermite-Gaussian modes. For example, if the X state in the  $\{|+\rangle, |-\rangle\}$  basis has been encoded in the polarization and OAM states of a photon pair, such that the first and last qubit are encoded in polarization states and the middle in the OAM state of one of the photons, the same state in the  $\{|H\rangle, |V\rangle\}$  and  $\{|h\rangle, |v\rangle\}$  basis would be  $\frac{1}{\sqrt{2}}(|HhH\rangle - i|VvV\rangle)$ .

We will consider the X state, the GHZ state, and a biased GHZ state in the  $\{|+\rangle, |-\rangle\}$  basis since this allows us to implement cyclic local  $SU(2)$  evolutions that reveal the topological phases and lie completely within the set of operators that diagonalize in the  $\{|+\rangle, |-\rangle\}$  basis. Considering the X state there are evolutions in each homotopy class that diagonalize in the  $\{|+\rangle, |-\rangle\}$  basis, and thus allows all possible topological phases to be observed. This is true also for the biased GHZ state.

### III. QUANTUM STATE PREPARATION

Our experimental proposal is based on the spontaneous parametric down conversion (SPDC) source of entangled photons first demonstrated in Ref. [23], and later used in other experiments [24, 25]. There, two adjacent nonlinear crystals cut for type I phase match are spatially oriented with their optical axis mutually orthogonal. Starting from a linearly polarized laser, a quarter waveplate (QWP-p) can be used to produce a circularly polarized pump, and generate pairs of polarization entangled photons of the kind

$$|\psi_{pol}\rangle = \frac{|HH\rangle - i|VV\rangle}{\sqrt{2}}, \quad (2)$$

where the first term on the right hand side comes from the  $V$  component of the pump while the second one comes from the  $H$  component.

In order to realize the three-qubit system, we may add the orbital angular momentum (OAM) quantum state of the photon pair [26]. As already demonstrated [27–29], the spatial correlations imposed by the phase match condition in parametric down conversion are manifested in the OAM transfer from the pump to the down converted photons, giving rise to an OAM entangled state of the form

$$|\psi_{oam}\rangle = \sum_m C_m |m, l-m\rangle, \quad (3)$$

where  $m$  and  $l$  are the topological charges of signal and pump photons, respectively. Then, OAM conservation imposes that the added topological charge of signal and idler equals that of the pump, leading to a superposition of all components compatible with this condition. The probability amplitudes  $C_m$  associated with a particular OAM partition is proportional to the spatial overlap between signal, idler, and pump transverse modes [30]. Now, the three-qubit realization can be achieved by pumping the SPDC source with a Laguerre-Gaussian mode with  $l = +1$  and detecting the idler photon with a single mode fiber (SMF) that admits only the  $l-m = 0$  component. Then, coincidence measurements should be obtained only for signal photons with  $m = +1$ . Therefore, the postselected spin-orbit quantum state is

$$|\psi_{SO}\rangle = |\psi_{pol}\rangle \otimes |+, 0\rangle. \quad (4)$$

Since the subspace of first order paraxial modes have a qubit structure [31], we can now encode two qubits on the signal photons, namely their polarization and OAM, and a single qubit on the idler polarization. From now on, we shall omit the idler OAM since no operations other than detection filtering will be performed in this degree of freedom. Therefore, the initial three-qubit state generated is

$$|\psi_1\rangle = \frac{|H+H\rangle - i|V+V\rangle}{\sqrt{2}}, \quad (5)$$

where we have grouped together the signal degrees of freedom. Now we shall discuss separately the two entangled three-qubit states of interest. We further show how to prepare certain product states that are used to investigate the role of entanglement in the topological phase measurements.

#### A. X State

First, we will see how to produce the three-qubit quantum state showing the  $\pi/2$  topological phase. The proposed setup is sketched in Fig. 1. In order to simply understand the setup, it is useful to recall that the X state in the  $\{|+\rangle, |-\rangle\}$  basis corresponds to a GHZ state in the  $\{|H\rangle, |V\rangle\}$  basis. Therefore, following the setup, we shall be seeking for this state. First, an astigmatic mode converter can be used to transform the signal LG mode to a horizontal first order HG mode [32], giving

$$|\psi_1\rangle \rightarrow |\psi_2\rangle = \frac{|HhH\rangle - i|VhV\rangle}{\sqrt{2}}. \quad (6)$$

This state could also be produced by pumping the crystals with the first order Hermite-Gaussian mode  $h$ , still filtering the idler with the single mode fiber. In this case, the signal mode with optimal spatial overlap with pump and idler is also  $h$ . This would exempt the use of the mode converter, making the system alignment considerably easier.

Then, a spin-orbit controlled NOT (CNOT) gate is used to flip the signal HG mode conditioned to its polarization. The CNOT gate is a Mach-Zehnder interferometer with input and output polarizing beam splitters (PBS). A Dove prism (DP) oriented at  $45^\circ$  and inserted in the ( $V$ ) arm makes the transverse mode conversion  $|h\rangle \rightarrow |v\rangle$  on this arm. After the CNOT gate the three-qubit quantum state becomes the desired X state:

$$\begin{aligned} |\psi_X\rangle &= \frac{|HhH\rangle - i|VvV\rangle}{\sqrt{2}} \\ &= \frac{|+++\rangle + |+-\rangle + |-+-\rangle + |--+\rangle}{2}. \end{aligned} \quad (7)$$

#### B. Biased GHZ state

In order to produce the biased GHZ state showing only topological phase  $\pi$ , the setup shown in Fig. 2 can be used. First, a half waveplate (HWP-p) with a suitable orientation is placed on the pump laser to set its polarization to produce the partially entangled state

$$|\psi'_{pol}\rangle = \alpha|HH\rangle + \beta|VV\rangle, \quad (8)$$

so that the initial three qubit state will be

$$|\psi'_1\rangle = \alpha|H+H\rangle + \beta|V+V\rangle. \quad (9)$$

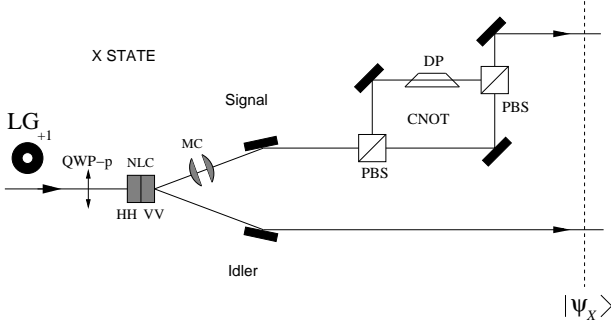


FIG. 1: X state preparation setup.

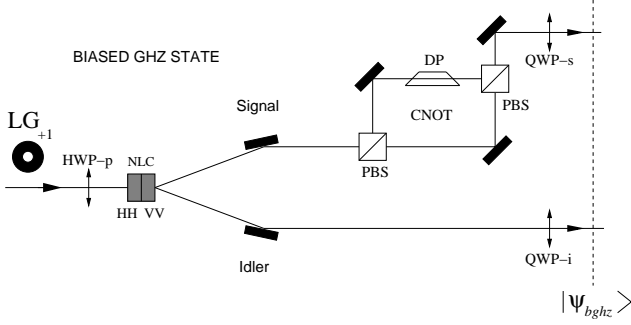


FIG. 2: Biased GHZ preparation setup.

With the astigmatic mode converter removed, the transformation  $|+\rangle \rightarrow |-\rangle$  is performed in the (V) arm of the CNOT gate, giving

$$|\psi'_2\rangle = \alpha|H+H\rangle + \beta|V-V\rangle. \quad (10)$$

Now, two quarter wave plates inserted on signal (QWP-s) and idler (QWP-i) paths, make the polarization transformations  $|H\rangle \rightarrow |+\rangle$  and  $|V\rangle \rightarrow |-\rangle$  needed to produce the desired biased GHZ state

$$|\psi_{bghz}\rangle = \alpha|+++\rangle + \beta|---\rangle. \quad (11)$$

### C. Product states

In order to investigate the role of entanglement in the topological phase measurements, it is important to compare the quantum states discussed above with product states that are equivalent to the X state and the biased GHZ state in what regards the single qubit probabilities.

For example, the product state

$$\begin{aligned} |\psi_{prod}\rangle &= \frac{|H\rangle + |V\rangle}{\sqrt{2}} \otimes \frac{|h\rangle + |v\rangle}{\sqrt{2}} \otimes \frac{|H\rangle + |V\rangle}{\sqrt{2}} \\ &= \frac{e^{-i\frac{\pi}{4}}|+\rangle + e^{i\frac{\pi}{4}}|-\rangle}{\sqrt{2}} \otimes \frac{e^{-i\frac{\pi}{4}}|+\rangle + e^{i\frac{\pi}{4}}|-\rangle}{\sqrt{2}} \\ &\quad \otimes \frac{e^{-i\frac{\pi}{4}}|+\rangle + e^{i\frac{\pi}{4}}|-\rangle}{\sqrt{2}} \end{aligned} \quad (12)$$

has the same probability distribution as the X state for each individual degree of freedom in both the  $\{|H\rangle, |V\rangle\}$  basis and the  $\{|+\rangle, |-\rangle\}$  basis.

This state is readily prepared by the setup shown in Fig. 3 when the pump polarization is set to V and the down converted photons are created at the product state  $|H+H\rangle$ . In the signal arm, the mode converter is then oriented to make the transformation  $|+\rangle \rightarrow (|h\rangle + |v\rangle)/\sqrt{2}$ , and the H polarization passes unaffected through the CNOT gate. Then, two half-waveplates can be used to set signal (HWP-s) and idler (HWP-i) polarizations to  $(|H\rangle + |V\rangle)/\sqrt{2}$ , thus producing  $|\psi_{prod}\rangle$ .

A product state with the same probability distributions as the biased GHZ state in the  $\{|+\rangle, |-\rangle\}$  basis could be

$$\begin{aligned} |\psi'_{prod}\rangle &= (\tilde{\alpha}|H\rangle + \tilde{\beta}|V\rangle) \otimes (\tilde{\alpha}|h\rangle + \tilde{\beta}|v\rangle) \\ &\quad \otimes (\tilde{\alpha}|H\rangle + \tilde{\beta}|V\rangle) \\ &= \frac{\alpha|+\rangle + \beta|-\rangle}{\sqrt{2}} \otimes \frac{\alpha|+\rangle + \beta|-\rangle}{\sqrt{2}} \\ &\quad \otimes \frac{\alpha|+\rangle + \beta|-\rangle}{\sqrt{2}}, \end{aligned} \quad (13)$$

where  $\tilde{\alpha} = \frac{\alpha+\beta}{\sqrt{2}}$  and  $\tilde{\beta} = i\frac{\alpha-\beta}{\sqrt{2}}$ .  $|\psi'_{prod}\rangle$  can be produced in the same way as  $|\psi_{prod}\rangle$ , but with suitable settings of the mode converter and the HWPs in order to provide the coefficients  $\tilde{\alpha}$  and  $\tilde{\beta}$ . Both  $|\psi_{prod}\rangle$  and  $|\psi'_{prod}\rangle$  could also be produced by tailoring the pump mode in order to optimize the spatial overlap between pump, idler, and the desired signal mode, without the use of a mode converter on the signal arm.

The role played by entanglement in the topological phase evolution can be investigated with two-photon interferometry, as we shall see in section V. The interference patterns produced by entangled states are clearly distinguished from those expected for product states.

## IV. TOPOLOGICAL PHASE MEASUREMENT

Under local unitary operations, the quantum state of the three-qubit photon pairs evolve keeping their entanglement unaltered. The topological nature of the phase evolution is strongly dependent on entanglement, so that it is important to identify entanglement signatures on the state evolution. As in Ref. [6], signatures of entanglement can be found on interference patterns between

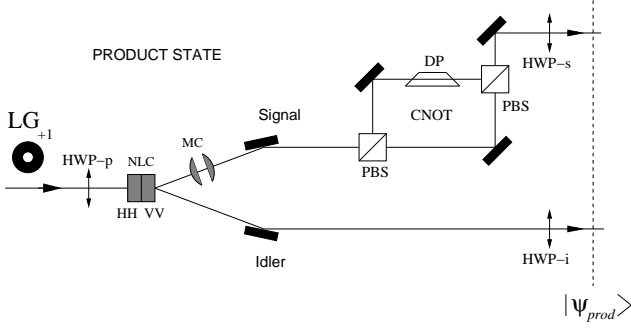


FIG. 3: Product state preparation setup.

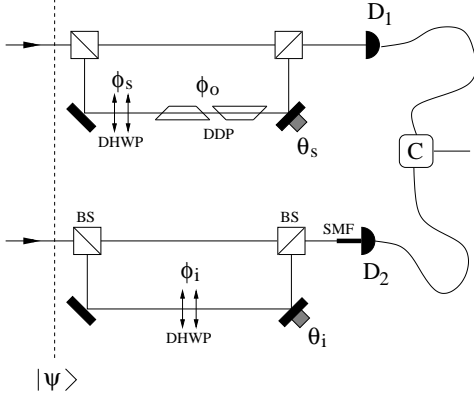


FIG. 4: Franson interferometry.

the evolved and the initial state. Two-photon interference can be achieved with the well known Franson setup, where each photon from a quantum correlated pair is sent through two alternative paths, a long and a short one [33–36]. When the delay time between the short and the long paths is larger than the detection time window, the two-photon coincidence count exhibits interference patterns. Each coincidence count may result from both photons following either the short or the long paths. Photons going through different paths do not coincide. Moreover, each arm of an SPDC source has a considerably short coherence length, so that no single photon interference can occur. Then, the overlap between the evolved and the initial state appears as the fringe visibility when the three qubits are individually operated in one arm and left unchanged in the other, as sketched in Fig. 4.

In order to simplify the experimental proposal, still being able to cover the topological structure of the three-qubit local  $SU(2)$  orbits, we shall be dealing with diagonal unitary operations in the  $\{|+\rangle, |-\rangle\}$  basis. For each polarization transformation, a sequence of two HWPs (DHWP) oriented at  $0$  and  $\phi$ , respectively, can be used. The same kind of diagonal transformation for OAM (LG basis) can be performed by a sequence of two DPs (DDP) at different orientations. These schemes are sketched in Fig. 4. It is instructive to view the operations performed

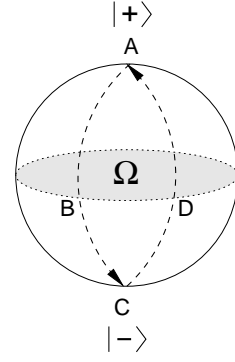


FIG. 5: Paths on the Poincaré sphere.

by the DHWPs and DDP in the single qubit Poincaré representation. Starting from a  $|+\rangle$  state, a HWP with its fast axis oriented at angle  $\theta$  makes the transformation  $|+\rangle \rightarrow |\theta + \pi/4\rangle \rightarrow |-\rangle$ , where  $|\theta\rangle$  represents a linear polarization state along a direction rotated by the angle  $\theta$  with respect to the horizontal. Therefore, a sequence of two HWPs oriented at  $\theta$  and  $\theta + \phi$ , respectively, makes the cycle  $|+\rangle \rightarrow |\theta + \pi/4\rangle \rightarrow |-\rangle \rightarrow |\theta + \phi + \pi/4\rangle \rightarrow |+\rangle$ , which corresponds to path  $A \rightarrow B \rightarrow C \rightarrow D \rightarrow A$  in Fig. 5. Since this path is composed of two geodesic segments, enclosing a solid angle  $\Omega = \phi$ , a purely geometric phase  $\phi/2$  is acquired by single qubits initially prepared at  $|+\rangle$ . Of course, the same solid would be enclosed by an initial state  $|-\rangle$ , but in opposite direction, giving a geometric phase  $-\phi/2$ . Therefore, each degree of freedom follows the local  $SU(2)$  operation:

$$U(\phi) = \begin{bmatrix} e^{i\phi/2} & 0 \\ 0 & e^{-i\phi/2} \end{bmatrix}, \quad (14)$$

given in the  $\{|+\rangle, |-\rangle\}$  basis, so that the overall three-qubit state will be transformed according to  $U(\phi_s) \otimes U(\phi_o) \otimes U(\phi_i)$ , where  $\phi_s$ ,  $\phi_o$ , and  $\phi_i$  correspond to signal polarization, OAM, and idler polarization, respectively.

Under these local operations, product and entangled states evolve differently in what regards the overlap between the initial and the evolved states:  $\langle\psi|U(\phi_s) \otimes U(\phi_o) \otimes U(\phi_i)|\psi\rangle$ . In order to access these differences and investigate the role played by entanglement and its relationship to the three-qubit topological structure, we must perform interferometric measurements where a proper background for comparison between product and entangled states can be established. A possible strategy is suggested in Fig. 4, where dynamical phases  $\theta_s$  and  $\theta_i$  are deliberately added in one arm of the interferometer. As these dynamical phases are continuously varied, the coincidence count exhibits an interference pattern that should evolve as the single qubit unitary operations are applied. In fact, the coincidence count is proportional to

$$C = C_0 [1 + \mathcal{V} \cos(\theta + \Phi)] , \quad (15)$$

where  $C_0$  is the coincidence offset,  $|\psi\rangle$  is one of the selected states discussed above,  $\theta = \theta_s + \theta_i$  is the total

dynamical phase added and

$$\begin{aligned}\Phi &\equiv \arg [\langle \psi | U(\phi_s) \otimes U(\phi_o) \otimes U(\phi_i) | \psi \rangle], \\ \mathcal{V} &\equiv |\langle \psi | U(\phi_s) \otimes U(\phi_o) \otimes U(\phi_i) | \psi \rangle|. \end{aligned} \quad (16)$$

Therefore, the absolute value of the overlap between the initial and the evolved states  $\mathcal{V}$  is related to the fringe visibility, while the overlap phase  $\Phi$ , i.e., the Pancharatnam relative phase [37, 38], translates to a fringe displacement. For a cyclic evolution, the fringes should recover maximal visibility and exhibit the accumulated phase shift, which is of topological nature for entangled states. However, the role of entanglement must be captured from signatures on the evolution of the interference pattern, as the individual unitary operations are applied. We shall investigate these signatures numerically in the next section.

## V. NUMERICAL RESULTS

To demonstrate the presence of the topological phases of the two different topological structures represented by the X state and the biased GHZ state we give examples of cyclic unitary evolutions in each homotopy class for both states. The evolution of the interference pattern for these entangled states, as the unitary evolution is gradually implemented, is compared to the evolution of the interference patterns of product states with the same local statistics in the  $\{|+\rangle, |-\rangle\}$  basis. Since we consider unitary evolutions that are diagonal in the  $\{|+\rangle, |-\rangle\}$  basis, no difference in the interference patterns between an entangled state and such a product state can be attributed to the local degrees of freedom. Any difference is thus due to entanglement.

### A. X state

A set of cyclic evolutions of the X state resulting in a  $\frac{\pi}{2}$  phase shift is generated by the unitary operators  $U(\phi_s(t)) \otimes U(\phi_o(t)) \otimes U(\phi_i(t))$ , where  $t \in [0, T]$ , such that  $\phi_s(0) = \phi_o(0) = \phi_i(0) = 0$  and  $\phi_s(T) = \phi_o(T) = \phi_i(T) = -\pi$ . For such an evolution of  $|\psi_X\rangle$ , the coincidence intensity  $C$  as a function of  $\theta, \phi_s, \phi_o$ , and  $\phi_i$  is given by the expression

$$\begin{aligned}C &= C_0 \left[ 1 + \frac{1}{2} \cos \left( \theta + \frac{\phi_s}{2} \right) \cos \left( \frac{\phi_o + \phi_i}{2} \right) \right. \\ &\quad \left. + \frac{1}{2} \cos \left( \theta - \frac{\phi_s}{2} \right) \cos \left( \frac{\phi_o - \phi_i}{2} \right) \right]. \end{aligned} \quad (17)$$

One unitary operator of this kind is  $U_{X1}(t)$  given by  $\phi_s(t) = \phi_o(t) = \phi_i(t) = -\pi t/T$ . If the X state is evolved by  $U_{X1}(t)$  the coincidence intensity as a function of  $t$  and  $\theta$  is given by

$$C(t, \theta) = C_0 \left[ 1 + \frac{1}{4} \cos \left( \theta - \frac{3\pi t}{2T} \right) + \frac{3}{4} \cos \left( \theta + \frac{\pi t}{2T} \right) \right]. \quad (18)$$

We can see that there is a reappearance of maximal fringe visibility for  $\frac{t}{T} = 1$  with the expected fringe shift  $\frac{\pi}{2}$ . Moreover, there are no values of  $\frac{t}{T}$  for which the interference fringes disappear. This illustrates that, in contrast to the case of maximally entangled two-qubit states [3], nontrivial topological phases can be obtained without going through a state orthogonal to the initial one. The coincidence intensity in Eq. (18) for selected values of  $\frac{t}{T}$  is shown in the left panel of Fig. 6.

Another cyclic evolution in the same homotopy class can be generated by the unitary operator  $U_{X2}(t)$  given by

$$\begin{aligned}\phi_s(t) &= -\pi - \pi \left[ \frac{3t}{T} - 1 \right] H \left[ \frac{1}{3} - \frac{t}{T} \right] \\ \phi_o(t) &= -\pi - \pi \left[ \left( \frac{3t}{T} - 1 \right) H \left( \frac{t}{T} - \frac{1}{3} \right) - 1 \right] H \left[ \frac{2}{3} - \frac{t}{T} \right] \\ \phi_i(t) &= -\pi - \pi \left[ \left( \frac{3t}{T} - 2 \right) H \left( \frac{t}{T} - \frac{2}{3} \right) - 1 \right], \end{aligned} \quad (19)$$

for  $0 \leq t \leq T$ , where  $H$  is the Heaviside step function defined by  $H(x) = 0$  for  $x < 0$  and  $H(x) = 1$  for  $x > 0$ . The coincidence intensity as a function of  $\theta$  and  $t$  in this case is

$$\begin{aligned}C(t, \theta) &= C_0 \left[ 1 + H \left( 1 - \frac{3t}{T} \right) \cos \theta \cos \left( \frac{3\pi t}{2T} \right) \right. \\ &\quad \left. + H \left( \frac{3t}{T} - 2 \right) \sin \theta \sin \left( \frac{3\pi t}{2T} \right) \right]. \end{aligned} \quad (20)$$

Again we can see the expected fringe shift  $\frac{\pi}{2}$  with maximal fringe visibility for  $\frac{t}{T} = 1$ . For the cyclic evolution generated by  $U_{X2}(t)$ , as opposed to that generated by  $U_{X1}(t)$ , the interference fringes disappear for  $\frac{1}{3} \leq \frac{t}{T} \leq \frac{2}{3}$ , meaning that the evolution takes the system through states orthogonal to the initial state during the evolution. With respect to the evolution of the fringe visibility there are thus qualitatively different evolutions in the same homotopy class. The coincidence intensity in Eq. (20) for selected values of  $\frac{t}{T}$  is shown in the left panel of Fig. 7.

To verify that the fringe shifts are due to entanglement we consider the product state  $|\psi_{prod}\rangle$ , defined in Eq. (12), which has the same probability distributions for the local degrees of freedom as the X state in both the  $\{|H\rangle, |V\rangle\}$  and the  $\{|+\rangle, |-\rangle\}$  bases. The coincidence intensity as a function of  $\theta, \phi_s, \phi_o$ , and  $\phi_i$  for  $|\psi_{prod}\rangle$ , given that it is subjected to a unitary  $U(\phi_s) \otimes U(\phi_o) \otimes U(\phi_i)$ , is

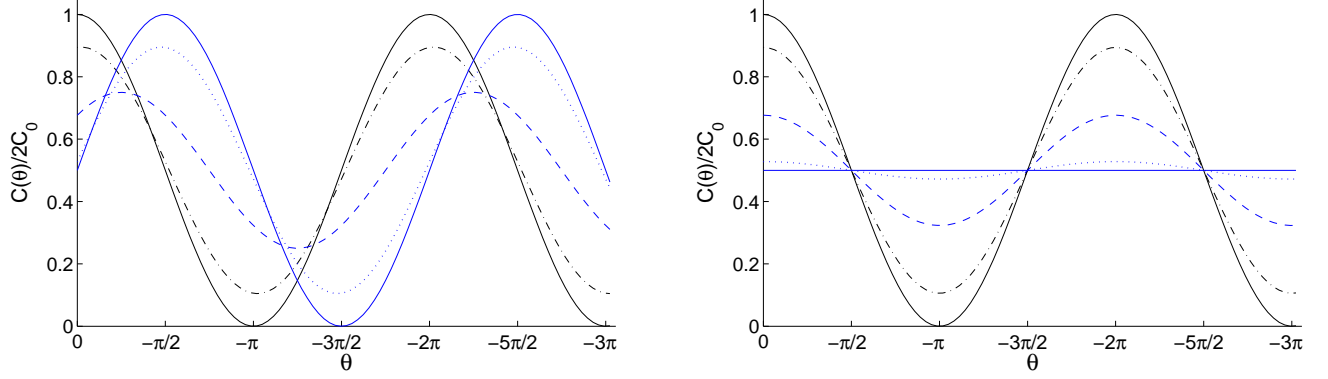


FIG. 6: (Color online) The coincidence intensity  $C(\theta)$  as a function of  $\theta$  for selected values of  $\frac{t}{T}$  of the evolution generated by  $U_{X1}(t)$  for  $|\psi_X\rangle$  (left) and  $|\psi_{prod}\rangle$  (right). The different interference intensities correspond to the values  $\frac{t}{T} = 0$  (solid black),  $\frac{t}{T} = \frac{1}{4}$  (dash-dotted black),  $\frac{t}{T} = \frac{1}{2}$  (dashed blue),  $\frac{t}{T} = \frac{3}{4}$  (dotted blue), and  $\frac{t}{T} = 1$  (solid blue), respectively.

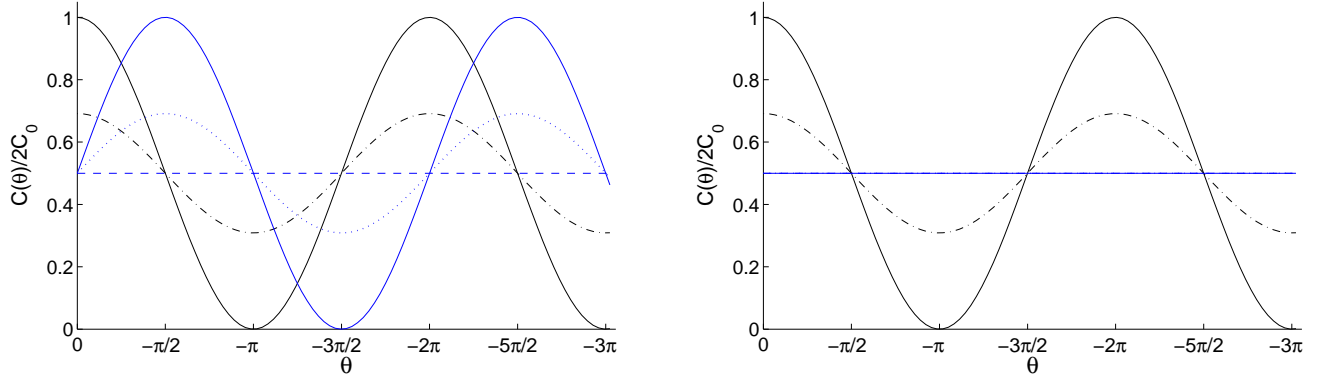


FIG. 7: (Color online) The coincidence intensity  $C(\theta)$  as a function of  $\theta$  for selected values of  $\frac{t}{T}$  of the evolution generated by  $U_{X2}(t)$  for  $|\psi_X\rangle$  (left) and  $|\psi_{prod}\rangle$  (right). The different interference intensities correspond to the values  $\frac{t}{T} = 0$  (solid black),  $\frac{t}{T} = \frac{1}{4}$  (dash-dotted black),  $\frac{t}{T} = \frac{1}{2}$  (dashed blue),  $\frac{t}{T} = \frac{3}{4}$  (dotted blue), and  $\frac{t}{T} = 1$  (solid blue), respectively.

$$C = C_0 \left[ 1 + \cos \theta \cos \left( \frac{\phi_s}{2} \right) \cos \left( \frac{\phi_o}{2} \right) \cos \left( \frac{\phi_i}{2} \right) \right]. \quad (21)$$

We can see that fringe visibility for  $\phi_s(T) = \phi_o(T) = \phi_i(T) = -\pi$  is zero. For  $|\psi_{prod}\rangle$  the only values of  $\phi_s, \phi_o$ , and  $\phi_i$  that gives maximal fringe visibility are 0 and  $2\pi$ . Thus, the reappearance of maximal fringe visibility for the value  $-\pi$  of  $\phi_s, \phi_o$  and  $\phi_i$  with a  $\frac{\pi}{2}$  fringe shift, is due to the entanglement of the X state. The coincidence intensity in Eq. (21) for the evolutions of  $|\psi_{prod}\rangle$  generated by  $U_{X1}(t)$  and by  $U_{X2}(t)$  at selected values of  $\frac{t}{T}$  is shown in the right panel of Figs. 6 and 7 respectively.

Note that the cyclic unitary evolutions that give maximal fringe visibility for  $|\psi_{prod}\rangle$  are also cyclic evolutions of the X state. This however holds only for the diagonal unitary operators we are considering. A more general cyclic evolution of  $|\psi_{prod}\rangle$  is not typically a cyclic evolution of  $|\psi_X\rangle$ .

The set of cyclic evolutions generating the  $\pi$ -phase shift of the X state that are diagonal in the  $\{|+\rangle, |-\rangle\}$

basis are the evolutions  $U(\phi_s(t)) \otimes U(\phi_o(t)) \otimes U(\phi_i(t))$   $t \in [0, T]$  such that  $\phi_s(0) = \phi_o(0) = \phi_i(0) = 0$  and  $\phi_s(T) = \phi_o(T) = \phi_i(T) = -2\pi$ . However since these are also cyclic evolutions of the product state  $|\psi_{prod}\rangle$  the reappearance of maximal fringe visibility and  $\pi$  phase shift cannot be attributed to the entanglement of the X state.

To observe a  $\pi$  phase shift that cannot be attributed to local degrees of freedom we must implement a cyclic evolution generated by unitaries that are not diagonal in the  $\{|+\rangle, |-\rangle\}$  basis. We recall however that the X state is identical to the GHZ state in a different basis. For the GHZ state there are evolutions generated by diagonal unitaries leading to a  $\pi$  phase shift that can be attributed to entanglement.

## B. GHZ and biased GHZ state

We consider the GHZ state  $|\psi_{ghz}\rangle = \frac{1}{\sqrt{2}}|++\rangle + \frac{1}{\sqrt{2}}|--\rangle$  and the biased GHZ state  $|\psi_{bghz}\rangle = \frac{1}{2}|++\rangle + \frac{1}{2}|--\rangle$

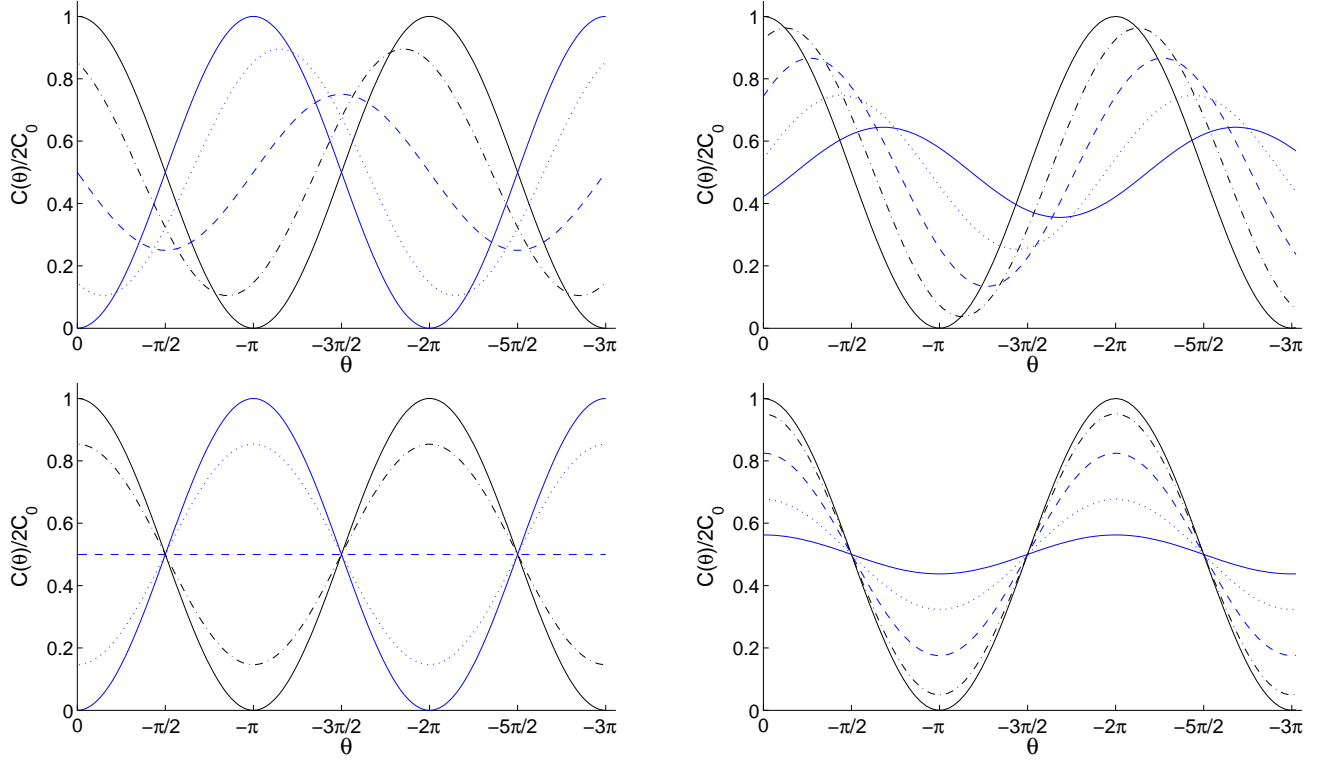


FIG. 8: (Color online) The coincidence intensity  $C(\theta)$  as a function of  $\theta$  for selected values of  $\frac{t}{T}$  of the evolution generated by  $U_{bghz}(t)$  for  $|\psi_{bghz}\rangle$  (upper left),  $|\psi'_{prod}\rangle$  (upper right),  $|\psi_{ghz}\rangle$  (lower left), and  $|\psi_{prod}\rangle$  (lower right). The different interference intensities correspond to the values  $\frac{t}{T} = 0$  (solid black),  $\frac{t}{T} = \frac{1}{4}$  (dash-dotted black),  $\frac{t}{T} = \frac{1}{2}$  (dashed blue),  $\frac{t}{T} = \frac{3}{4}$  (dotted blue), and  $\frac{t}{T} = 1$  (solid blue), respectively.

$++\rangle + \frac{\sqrt{3}}{2}|--\rangle$ . The GHZ state and the biased GHZ state share a set of cyclic evolutions that give rise to a  $\pi$  phase shift and are diagonal in the  $\{|+\rangle, |-\rangle\}$  basis. We recall however that the GHZ state and the biased GHZ state are representatives of different classes of topological phase structures of the local  $SU(2)$  orbits since for the GHZ state there are cyclic evolutions resulting in a  $\frac{\pi}{2}$  phase shift while for the biased GHZ state there are no such evolutions.

The cyclic evolutions of these states that result in a  $\pi$  phase shift are generated by unitaries  $U(\phi_s(t)) \otimes U(\phi_o(t)) \otimes U(\phi_i(t))$ , where  $t \in [0, T]$ , such that  $\phi_s(0) = \phi_o(0) = \phi_i(0) = 0$ , and  $\phi_1(T) + \phi_2(T) + \phi_3(T) = \pm 2\pi$ . There are no evolutions generated by unitaries of this kind that takes the biased GHZ state through a state orthogonal to the initial state. Thus, the interference fringes never disappears. The GHZ state on the other hand is evolved through an orthogonal state.

One unitary operator of this kind is  $U_{bghz}(t)$  given by the choice  $\phi_s(t) = \phi_o(t) = \phi_i(t) = \frac{2\pi t}{3T}$ . The coincidence intensity for the evolution of  $|\psi_{ghz}\rangle$  generated by  $U_{bghz}(t)$  will be a function of  $t$  and  $\theta$  given by

$$C(t, \theta) = C_0 \left[ 1 + \cos \theta \cos \left( \frac{\pi t}{T} \right) \right]. \quad (22)$$

The coincidence intensity in Eq. (22) for selected values

of  $\frac{t}{T}$  is shown in the lower left panel of Fig. 8. The coincidence intensity for the evolution of  $|\psi_{bghz}\rangle$  generated by  $U_{bghz}(t)$  on the other hand will include an additional term and is given as a function of  $t$  and  $\theta$  by

$$C(t, \theta) = C_0 \left[ 1 + \cos \theta \cos \left( \frac{\pi t}{T} \right) - \frac{1}{2} \sin \theta \sin \left( \frac{\pi t}{T} \right) \right]. \quad (23)$$

The coincidence intensity in Eq. (23) for selected values of  $\frac{t}{T}$  is shown in the upper left panel of Fig. 8. For both the GHZ state and the biased GHZ state the coincidence intensity depends only on the sum  $\phi_s(t) + \phi_o(t) + \phi_i(t)$  and not on the  $\phi_i(t)$  individually. For both states there is a reappearance of maximal fringe visibility at  $\frac{t}{T} = 1$  and the interference fringes are shifted by a  $\pi$  phase.

To see the signature of the entanglement in the interference pattern of  $|\psi_{bghz}\rangle$ , we also consider the product state

$$\begin{aligned} |\psi'_{prod}\rangle &= \left( \frac{1}{2}|+\rangle + \frac{\sqrt{3}}{2}|-\rangle \right) \otimes \left( \frac{1}{2}|+\rangle + \frac{\sqrt{3}}{2}|-\rangle \right) \\ &\otimes \left( \frac{1}{2}|+\rangle + \frac{\sqrt{3}}{2}|-\rangle \right), \end{aligned} \quad (24)$$



which has the same probability distributions for the local degrees of freedom in the  $\{|+\rangle, |-\rangle\}$  basis as  $|\psi_{bghz}\rangle$ . The interference intensity as a function of  $\theta$  and  $t$  when  $|\psi'_{prod}\rangle$  is evolved by  $U_{bghz}(t)$  is

$$C(t, \theta) = C_0 \left\{ 1 + \cos \theta \cos \left[ \frac{\pi t}{3T} \right] \left[ 1 - \frac{7}{4} \sin^2 \left( \frac{\pi t}{3T} \right) \right] + \frac{3}{2} \sin \theta \sin \left[ \frac{\pi t}{3T} \right] \left[ 1 - \frac{13}{12} \sin^2 \left( \frac{\pi t}{3T} \right) \right] \right\}. \quad (25)$$

Comparing Eqs. (23) and (25) we see that the reappearance of maximal fringe visibility for  $\frac{t}{T} = 1$  is absent for  $|\psi'_{prod}\rangle$ . Moreover the fringe shift is not equal to  $\pi$ . Thus, the reappearance of fringe visibility and  $\pi$  phase shift is thus due to entanglement. The coincidence intensity for  $|\psi'_{prod}\rangle$ , evolved by  $U_{bghz}$ , is shown for selected values of  $\frac{t}{T}$  in upper right panel of Fig. 8 alongside the coincidence intensity of  $|\psi_{bghz}\rangle$ .

To see the signature of entanglement in the interference pattern of  $|\psi_{ghz}\rangle$  in Eq. (22) we compare with the interference patterns of  $|\psi_{prod}\rangle$ . The coincidence intensity for  $|\psi_{prod}\rangle$  is given by Eq. (21) and we can see that there is no reappearance of maximal fringe visibility for  $\phi_s(t) = \phi_o(t) = \phi_i(t) = \frac{2\pi}{3}$ . Thus, the reappearance for  $|\psi_{bghz}\rangle$  can be attributed to entanglement and the phase shift is of topological nature. The coincidence intensity for  $|\psi_{prod}\rangle$ , evolved by  $U_{bghz}$ , is shown for selected values of  $\frac{t}{T}$  in the lower right panel of Fig. 8 alongside the coincidence intensity for  $|\psi_{ghz}\rangle$ .

## VI. CONCLUSIONS

We propose an experimental scheme to observe the topological phases acquired by special classes of three-qubit states. These phases reveal the nontrivial topological structure of the local  $SU(2)$  orbits. In particular, observation of the  $\pi/2$  topological phase shift would be a signature of multiqubit entanglement as this phase exists only for more than two qubits. The experimental proposal is within the technological resources available in most quantum optics laboratories, and can be implemented in a short term. Furthermore, the insensitivity to continuous path deviations of the unitary evolution is a robust feature of the topological phases with potential applications to quantum information processing.

## Acknowledgments

M.J., E.S., and K.S. acknowledge support from the National Research Foundation and the Ministry of Education (Singapore). A. Z. Khoury acknowledges funding from the Brazilian agencies Coordenação de Aperfeiçoamento de Pessoal de Nível Superior (CAPES), Fundação de Amparo à Pesquisa do Estado do Rio de Janeiro (FAPERJ-BR), and Conselho Nacional de Desenvolvimento Científico e Tecnológico (CNPq). A. Z. Khoury is deeply grateful for the hospitality during the visit to Centre for Quantum Technologies at the National University of Singapore, Singapore.

- 
- [1] Y. Aharonov and D. Bohm, Phys. Rev. **115**, 485 (1959).
  - [2] P. Milman and R. Mosseri, Phys. Rev. Lett. **90**, 230403 (2003).
  - [3] P. Milman, Phys. Rev. A **73**, 062118 (2006).
  - [4] M. Kuś and K. Życzkowski, Phys. Rev. A **63**, 032307 (2001).
  - [5] R. Mosseri and R. Dandoloff, J. Phys. A **34**, 10243 (2003).
  - [6] C. E. R. Souza, J. A. O. Huguenin, P. Milman, and A. Z. Khoury, Phys. Rev. Lett. **99**, 160401 (2007).
  - [7] J. Du, J. Zhu, M. Shi, X. Peng, and D. Suter, Phys. Rev. A **76**, 042121 (2007).
  - [8] L. E. Oxman and A. Z. Khoury, Phys. Rev. Lett. **106**, 240503 (2011).
  - [9] M. Johansson, M. Ericsson, K. Singh, E. Sjöqvist, and M. S. Williamson, Phys. Rev. A **85**, 032112 (2012).
  - [10] V. Coffman, J. Kundu, and W. K. Wootters, Phys. Rev. A **61**, 052306 (2000).
  - [11] E. Nagali, F. Sciarrino, F. De Martini, L. Marrucci, B. Piccirillo, E. Karimi, and E. Santamato, Phys. Rev. Lett. **103**, 013601 (2009).
  - [12] E. Nagali, F. Sciarrino, F. De Martini, B. Piccirillo, E. Karimi, L. Marrucci, and E. Santamato, Opt. Express **17**, 18745 (2009).
  - [13] E. Karimi, S. Slussarenko, B. Piccirillo, L. Marrucci, and E. Santamato, Phys. Rev. A **81**, 053813 (2010).
  - [14] C. E. R. Souza and A. Z. Khoury, Opt. Express **18**, 9207 (2010).
  - [15] C. E. R. Souza, C. V. S. Borges, A. Z. Khoury, J. A. O. Huguenin, L. Aolita, and S. P. Walborn, Phys. Rev. A **77**, 032345 (2008).
  - [16] L. Chen and W. She, J. Opt. Soc. Am. B, **27**, A7 (2010).
  - [17] C. V. S. Borges, M. Hor-Meyll, J. A. O. Huguenin, and A. Z. Khoury, Phys. Rev. A **82**, 033833 (2010).
  - [18] W. Dür, G. Vidal, and J. I. Cirac, Phys. Rev. A **62**, 062314 (2000).
  - [19] A. Sudbery, J. Phys. A: Math Gen. **34**, 643 (2001).
  - [20] H. A. Carteret and A. Sudbery, J. Phys. A: Math. Gen. **33**, 4981 (2000).
  - [21] H. A. Carteret, A. Higuchi, and A. Sudbery, J. Math. Phys. **41**, 7932 (2000).
  - [22] A. Osterloh and J. Siewert, New J. Phys. **12**, 075025 (2010).
  - [23] P. G. Kwiat, E. Waks, A. G. White, I. Appelbaum, and P. H. Eberhard, Phys. Rev. A **60**, R773 (1999).
  - [24] M. França Santos, P. Milman, A. Z. Khoury, and P. H. Souto Ribeiro, Phys. Rev. A **64**, 023804 (2001).
  - [25] D. P. Caetano, P. H. Souto Ribeiro, J. T. C. Parda, and A. Z. Khoury, Phys. Rev. A **68**, 023805 (2003).
  - [26] M. J. Padgett and L. Allen, Opt. Comm. **121**, 36 (1995).

- [27] A. Mair, A. Vaziri, G. Weihs, and A. Zeilinger, *Nature* **412**, 313 (2001).
- [28] D. P. Caetano, M. P. Almeida, P. H. Souto Ribeiro, J. A. O. Huguenin, B. Coutinho dos Santos, and A. Z. Khoury, *Phys. Rev. A* **66**, 041801 (2002).
- [29] M. Martinelli, J. A. O. Huguenin, P. Nussenzveig, and A. Z. Khoury, *Phys. Rev. A* **70**, 013812 (2004).
- [30] C. I. Osorio, G. Molina-Terriza, and J. P. Torres, *Phys. Rev. A* **77**, 015810 (2008).
- [31] M. J. Padgett and J. Courtial, *Opt. Lett.* **24**, 430 (1999).
- [32] L. Allen, M. W. Beijersbergen, R. J. C. Spreeuw, and J. P. Woerdman, *Phys. Rev. A* **45**, 8185 (1992).
- [33] J. D. Franson, *Phys. Rev. Lett.* **62**, 2205 (1989).
- [34] J. D. Franson, *Phys. Rev. A* **44**, 4552 (1991).
- [35] L. C. B. Ryff, *Phys. Rev. A* **48**, 1020 (1993).
- [36] B. Hessmo and E. Sjöqvist, *Phys. Rev. A* **62**, 062301 (2000).
- [37] S. Pancharatnam, *Proc. Indian Acad. Sci., Sect. A* **44**, 247 (1956).
- [38] A.G. Wagh, V.C. Rakhecha, *Phys. Lett. A* **197**, 112 (1995).